First-Principles Studies of the Structural and Electronic Properties of the $(Ga_{1-x}Zn_x)(N_{1-x}O_x)$ Solid Solution Photocatalyst

Lin Lin Jensen,[‡] James T. Muckerman,*[,†] and Marshall D. Newton[†]

Chemistry Department, Brookhaven National Laboratory, Upton, New York 11973-5000, and Department of Chemistry, Penn State University, State College, Pennsylvania 16803

Received: May 9, 2007; In Final Form: October 1, 2007

Design of visible-light-driven photocatalytic materials has attracted intense interest in recent years in an attempt to enhance photonic efficiencies of hydrogen production via water splitting. Recent studies have shown that a solid solution of GaN and ZnO, $(Ga_{1-x}Zn_x)(N_{1-x}O_x)$, can oxidize water under visible light in the presence of a sacrificial electron acceptor. Here we present a systematic study of the structural and electronic properties of this $(Ga_{1-x}Zn_x)(N_{1-x}O_x)$ solid solution as a function of zinc (oxygen) concentration, x, using density-functional theory (DFT). The DFT+U approach has been adopted, and two different periodic supercells, the 16-atom $(Ga_{8-n}Zn_n)(N_{8-n}O_n)$ and 32-atom $(Ga_{16-n}Zn_n)(N_{16-n}O_n)$, have been used to model this solid solution. Results obtained from both supercells are in qualitative agreement with available experimental findings (in the lower concentration range $x < 0.25$), although overall the larger 32-atom supercell provides a better description of the $(Ga_{1-x}Zn_x)(N_{1-x}O_x)$ solid solution. Downward bowing of the band gap over the entire composition range has been observed for both supercells, and the minimum "experimental" band gap is estimated to be about 2.29 eV for the intermediate concentration $x = 0.525$. This suggests that the photocatalytic activity of this solid solution can be improved further by increasing its zinc (oxygen) concentration.

Introduction

Photocatalytic splitting of water into hydrogen and oxygen using solar energy has attracted substantial interest in recent years as a potentially clean and renewable source for hydrogen fuel.[1] Many photocatalysts suitable for water splitting have been developed; however, most of them operate only with ultraviolet light,[2−4] which accounts for only 4% of the solar spectrum. To enhance the light-absorption efficiency, considerable effort has been invested in developing visible-light-driven photocatalysts.[5−8] Recently, a solid solution of GaN and ZnO, $(Ga_{1-x}Zn_x)(N_{1-x}O_x)$, has been reported to be a stable photocatalyst that is capable of water splitting under visible light.[9,10]

Compared to its wide-gap components (GaN and ZnO, ~3.4 eV), the photocatalyst $(Ga_{1-x}Zn_x)(N_{1-x}O_x)$ has a narrower band gap (<3.0 eV) in the visible-light region. Similar to pure GaN and ZnO, $(Ga_{1-x}Zn_x)(N_{1-x}O_x)$ has a single-phase hexagonal wurtzite-type crystal structure, although the positions of its constituent atoms are still unknown.[11] The lattice constants, band gap, and the overall activity of this photocatalyst for water splitting have been shown to depend strongly on the zinc concentration, x;[12] however, the x range studied experimentally is quite limited ($x < 0.25$) and the nature of the observed band gap narrowing is not well understood. A better characterization of the composition dependence of the physical and optical properties of this material and a detailed understanding of the band gap-narrowing mechanism are necessary to further the design of optimal photocatalysts.

In this paper, we present a systematic study on the variation of the structural and electronic properties of the $(Ga_{1-x}Zn_x)(N_{1-x}O_x)$ solid solution with the Zn (O) concentration, x, by using density functional theory (DFT). Both pure components (GaN and ZnO) have been the subjects of detailed theoretical and experimental studies;[13−17] however, to our knowledge, theoretical studies on their solid solutions have not yet been reported. The major challenge of this study concerns the arrangement of the constituent atoms in the solid solution at different concentrations, x. The most direct approach is to construct a large supercell and occupy the sites of the supercell randomly to yield the desired composition. However, this approach can be computationally prohibitive because the supercell must necessarily be large to reproduce the characteristics of a random solution. Zunger et al.[18] have proposed a special quasirandom structure (SQS) approach in which special small-unit-cell periodic structures are constructed to closely mimic the most important structural features of the corresponding random solution. This approach can be incorporated into different first-principles techniques easily, and it has been used extensively to study properties of fcc-based,[18−20] bcc-based,[21] and hcp-based substitutional alloys.[20,22] In this study, we have employed this SQS approach and conducted an exhaustive search to determine the most energetically favorable configuration of the solid solution at several discrete levels of concentration, x.

A second key issue is that the standard DFT calculations based on the local density (LDA) or the generalized gradient approximation (GGA) generally underestimate the band gap of wide-gap semiconductors. Previous studies[13,23,24] have shown that in both GaN and ZnO the band gap predominantly results from interactions between the anion 2p states and the cation 4s states. The cation 3d states couple strongly (especially for ZnO) with the anion 2p states, pushing up the valence-band maximum and leading to an underestimation of the calculated band gap. These strong 2p−3d couplings present a particularly difficult challenge for standard DFT-LDA and DFT-GGA calculations and thus complicate the calculations of the electronic properties of the $(Ga_{1-x}Zn_x)(N_{1-x}O_x)$ solid solutions from the outset. Several developments have been made to treat these strong

* Corresponding author. E-mail: muckerma@bnl.gov.
[†] Brookhaven National Laboratory.
[‡] Penn State University.

10.1021/jp073554y CCC: $40.75
Published on Web 02/12/2008

couplings, among them, the LDA+U (or GGA+U) approach,[25−27] the self-interaction corrected pseudo-potential method (pseudo-SIC),[28] and the quasiparticle GW approximation method.[29] In this study, we have adopted the GGA+U approach to study the $(Ga_{1-x}Zn_x)(N_{1-x}O_x)$ solid solution and our results are in qualitative agreement with experimental findings.

Model and Method

Model Structures. The properties of the $(Ga_{1-x}Zn_x)(N_{1-x}O_x)$ solid solution at a given Zn (O) concentration, x, are dependent on the atomic configuration, that is, the arrangement of the substitutional atoms (Ga and Zn) or (N and O) on the lattice sites. To find the most stable configuration of this solid solution at a given x, we have first started from a 16-atom $(Ga_{8-n}Zn_n)(N_{8-n}O_n)$ ($n = 0,...,8$) supercell, which corresponds to a $2 \times 2 \times 1$ supercell that is twice the size of the primitive wurtzite unit cell in both directions of the basal plane. The small size of this supercell allows us to sample every possible atomic configuration at each (discrete) Zn (O) concentration for the entire composition region.

However, this 16-atom $(Ga_{8-n}Zn_n)(N_{8-n}O_n)$ supercell is likely to be too small to represent the random solid solution adequately. The wurtzite structure of the $(Ga_{1-x}Zn_x)(N_{1-x}O_x)$ solid solution is made of two hcp sublattices, with one occupied solely by the cation $(Ga_{1-x}Zn_x)$ atoms and the other by the anion $(N_{1-x}O_x)$ atoms. The two sublattices are related by an internal parameter u along the c axis but can be treated separately as hcp binary $A_{1-x}B_x$ alloys. The special quasirandom structures (SQS) approach proposed by Zunger et al.[18] has been used extensively to study the properties of $A_{1-x}B_x$ substitutional alloys. Recent studies by Liu et al.[22] have shown that 16-atom SQSs are capable of mimicking the most important structural features of the hcp alloys for composition at 25% (75%) and 50%. The basic idea of the SQS approach is to construct special small-unit-cell periodic structures that possess the first few pair- and multisite correlation functions that match the corresponding perfect random solution,[21,22] that is

$$(\bar{\Pi}_{k,m})_{\mathrm{SQS}} \cong \langle \bar{\Pi}_{k,m} \rangle_{\mathrm{R}} = (2x-1)^k \qquad (1)$$

where $\langle \bar{\Pi}_{k,m} \rangle_{\mathrm{R}}$ is the correlation function of a random alloy and x is its composition; $k = 1, 2, 3, ...$, corresponds to a cluster type (point, pair, triplet, ..., respectively); and $m = 1, 2, 3, ...$, denotes the first, second, and third-nearest neighbor, and so forth.

To study the effect of different supercell sizes and to better represent the important characteristics of the $(Ga_{1-x}Zn_x)(N_{1-x}O_x)$ random solid solution, we have adopted this SQS approach and considered a larger 32-atom $(Ga_{16-n}Zn_n)(N_{16-n}O_n)$ ($n = 0,...,16$) supercell. The lattice parameters of the unrelaxed 32-atom supercell are twice those of pure GaN bulk values, and the atomic positions of the cations $(Ga_{16-n}Zn_n)$ and anions $(N_{16-n}O_n)$ correspond, respectively, to the fractional coordinates of the 16 Ga and 16 N atoms in the $2 \times 2 \times 2$ GaN wurtzite lattice. A two-step procedure has been adopted to generate special structures to represent the $(Ga_{1-x}Zn_x)(N_{1-x}O_x)$ solid solution. First, the Alloy-Theoretic Automated Toolkit (ATAT)[30] is used to generate all possible structures for both cation and anion 16-atom hcp sublattices at Zn (O) concentrations $x = 0.25$, 0.5, and 0.75. For each structure, we have calculated the corresponding correlation functions $\bar{\Pi}_{k,m}$ and compared them with $\langle \bar{\Pi}_{k,m} \rangle_{\mathrm{R}}$ to obtain the structure(s) with the best match at concentration x. Second, the special cation and anion structures obtained at a given concentration, x, are combined to form the 32-atom model structure(s). The underlying constraint for this combination procedure is that the formation of nearest neighbor Ga−N and Zn−O pairs is the energetically most favorable in the solid solution. At the low $x = 1/16$ (and high $x = 15/16$) concentration limit, the "impurity supercell" with only one Zn−O or Ga−N pair per cell is adopted and two different atomic configurations have been considered: configuration C_a with O (N) being the first-nearest-neighbor above Zn (Ga) atoms and configuration C_b with O (N) being the first-nearest-neighbor below Zn (Ga) atoms, along the c axis.

For both the 16-atom $(Ga_{8-n}Zn_n)(N_{8-n}O_n)$ ($n = 0,...,8$) and the 32-atom $(Ga_{16-n}Zn_n)(N_{16-n}O_n)$ ($n = 0,...,16$) supercells, we have used the generated, unrelaxed model structures as initial geometrical input for the first-principles calculations outlined below. For each structure considered, the volume and shape of the supercell as well as the atomic positions have been fully relaxed and optimized. The most stable configuration at a given Zn (O) concentration, x, has been determined through the calculation of cohesive energies, for example

$$-E_{\mathrm{coh}} = \frac{E_{\mathrm{solid}} - \sum_A N_A E_A^{\mathrm{isolated}}}{N_{\mathrm{F.U.}}} \qquad (2)$$

where A represents different atoms that constitute the solid solution, N_A the number of A atoms, and $N_{\mathrm{F.U.}}$ the number of formula units in the supercell. For the two supercells considered here, the formula unit is defined as $(Ga_{1-x}Zn_x)(N_{1-x}O_x)$ with $x = n/8$ and $n/16$, respectively.

GGA+*U* Method. For most of the results presented here, we have used the projector-augmented wave (PAW) pseudopotential basis[31] with the Perdew−Burke−Ernzerhof (PBE)[32] version of the GGA exchange-correlation functional,[33] as implemented in the Vienna Ab initio Simulation Package.[34] The energy cutoff is set at 500 eV for all systems studied here, and the force on each atom is converged to 0.01 eV/Å for all structural relaxations. The 4s, 4p, and 3d electrons of Ga and Zn, and the 2p and 2s electrons of N and O are treated as valence electrons. A set of $5 \times 5 \times 4$ non-shifted Γ-centered special k-points has been used for the Brillouin zone integration for the 16-atom $(Ga_{8-n}Zn_n)(N_{8-n}O_n)$ supercell. For the 32-atom $(Ga_{16-n}Zn_n)(N_{16-n}O_n)$ supercell, we have first used a set of $4 \times 4 \times 3$ non-shifted Γ-centered special k-points for structural relaxations to search for the most stable configurations. A larger set of $5 \times 5 \times 3$ non-shifted Γ-centered special k-points has then been used for these optimized configurations to obtain more accurate energies and charge densities (for electronic band structure calculations). Different cutoff energies and k-point mesh sets have also been tested, and the present parameters are sufficient in obtaining well-converged total energy and geometrical configurations. For cohesive energy calculations, the energies of isolated Ga, Zn, N, and O atoms, with spin polarization, have been calculated by arranging them on a simple cubic supercell with lattice parameter of 12 Å.

An adequate description of the semicore 3d states of Ga and Zn is essential to study the electronic properties of the $(Ga_{1-x}Zn_x)(N_{1-x}O_x)$ solid solution. We have adopted the GGA+U approach, where U is the on-site Coulomb interaction correction. An important issue within this approach is the choice of the parameter U. This orbital-dependent parameter can in principle be calculated based on first-principles atomic calculations,[35,36] but in practice it is often treated as an empirical parameter.[27,37,38] We have introduced the U correction via the Dudarev formulation[39] implemented in VASP. The only free parameter in this

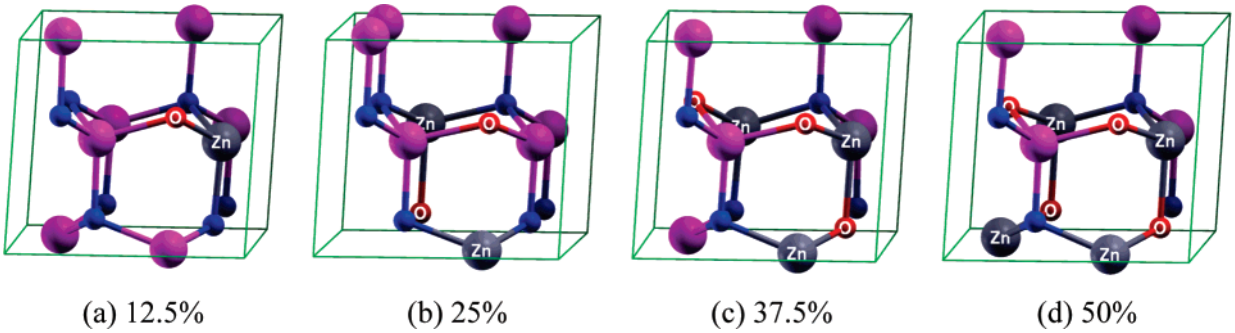

Figure 1. Most stable configurations of the 16-atom $(Ga_{8-n}Zn_n)(N_{8-n}O_n)$ supercell at different Zn (O) concentrations: Ga (purple), N (blue), Zn (gray), and O (red).

TABLE 1: Lattice Constant *a* (in Å), Axial Ratio *c*/*a*, Internal Parameters *u*, and Band Gaps E_g (in eV) of Wurtzite GaN and ZnO

	GaN				ZnO				
$\bar{U}-\bar{J}$	0.0	3.9	6.0	exp	0.0	4.7	6.0	8.0	exp
a	3.216	3.159	3.114	3.190[a]	3.288	3.241	3.222	3.192	3.249[b]
c/*a*	1.628	1.627	1.627	1.627[a]	1.613	1.610	1.610	1.608	1.602[b]
u	0.377	0.377	0.377	0.377[a]	0.381	0.381	0.381	0.381	0.383[b]
E_g	1.746	2.446	2.795	3.4[c]	0.732	1.376	1.568	1.889	3.2[c]

[a] References 14 and 40. [b] References 41 and 42. [c] Reference 12.

formulation is the difference between the effective Coulomb and the effective exchange interactions $\bar{U}-\bar{J}$. We have first tested several different $\bar{U}-\bar{J}$ values chosen from both first-principles results (3.9 eV for Ga and 4.7 eV for Zn 3d electrons)[35] and empirical parameters used previously.[27,38] Values that give the best overall agreement with experiment are then used throughout the calculations for both supercells.

Results and Discussions

Pure Components: GaN and ZnO. Table 1 lists the optimized structural properties and band gaps of wurtzite GaN and ZnO bulk solids using different values of $\bar{U}-\bar{J}$. The corresponding experimental values are also collected here. For both GaN and ZnO, we see that the lattice parameters decrease as the $\bar{U}-\bar{J}$ value increases. This is because the *U* correction makes the 3d states more localized and thus results in smaller lattice parameters.[35] Moreover, the band structures and the total density-of-states (DOS) plots (not shown here) show that as the $\bar{U}-\bar{J}$ value increases the band gap increases and the positions of the 3d states of both Ga and Zn shift downward. Our calculated GGA band gaps show the usual underestimation, only about 25% of experimental values for ZnO[13,23,24] and 50% for GaN.[24] The inclusion of the *U* correction improves the description of the semicore 3d states and the band gap in both GaN and ZnO, although one should not expect this approach to completely heal the DFT deficiency in underestimating band gaps. Comparing with experiments, we found that $\bar{U}-\bar{J}=3.9$ eV for Ga 3d[35] and 6.0 eV for Zn 3d[38] electrons give the best overall description regarding lattice parameters, band gaps, and band positions. We have thus applied these two values to all of the model structures considered for the $(Ga_{1-x}Zn_x)(N_{1-x}O_x)$ solid solution.

16-Atom $(Ga_{8-n}Zn_n)(N_{8-n}O_n)$ Supercell. We have conducted an exhaustive search at each (discrete) level of Zn (O) concentration, *x*, from 0 to 1 to determine the most stable structures of the 16-atom $(Ga_{8-n}Zn_n)(N_{8-n}O_n)$ supercell. Figure 1 shows the configurations of these structures at $x=0.125$, 0.25, 0.375, and 0.5. Configurations of the supercell with higher Zn (O) concentrations, $x=0.625$, 0.75, and 0.875 (not shown here), can be obtained approximately by switching the Ga and Zn atoms and the N and O atoms in the structures with complementary *x* values ($x=0.375$, 0.25, and 0.125, respectively). At the low $x=0.125$ (and high $x=0.875$) concentration limits, the C_a configuration (with the anion being above the first-nearest-neighbor cation along the *c* axis) is found to be energetically more favorable (~0.1 eV) than the C_b configuration. Moreover, configurations with the formation of nearest-neighbor Ga−N or Zn−O pairs are found to be energetically more favorable (~0.5 eV) than those with longer-range pairs.

Figure 2 shows the variations of the lattice parameters *a* (squares, scale at left) and *c* (circles, scale at right) of the scaled unit cell (corresponding to the primitive cell) with Zn (O) concentration, *x*, for the 16-atom $(Ga_{8-n}Zn_n)(N_{8-n}O_n)$ supercell. The scaled unit cell is defined here as a cell containing a total of four atoms, that is, the number of atoms in the primitive cell of GaN and ZnO. The corresponding cohesive energies per formula unit are shown in the inset. The gray straight lines represent ideal solution behavior, that is, the linear interpolation of the pseudo-binaries (GaN) and (ZnO). The solid and dashed lines connecting consecutive points are curves interpolated with cubic splines.

As can be seen from Figure 2 (inset), the calculated cohesive energy E_{coh} shows a nearly linear variation versus Zn (O) concentration, *x*, indicating that there is no driving force for

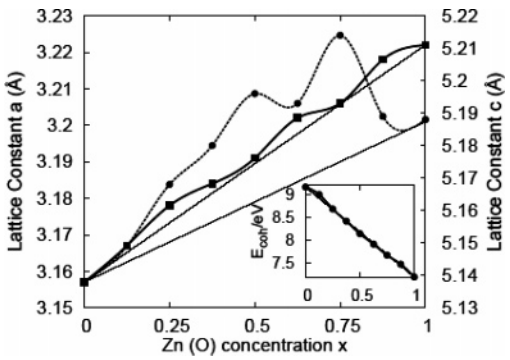

Figure 2. Calculated lattice parameters *a* (squares, scale at left) and *c* (circles, scale at right) of the scaled unit cell for the $(Ga_{8-n}Zn_n)(N_{8-n}O_n)$ supercell as a function of Zn (O) concentration, *x*. The inset shows the corresponding cohesive energies per formula unit at each *x*.

TABLE 2: Pair Correlation Functions up to the Fifth Neighbors of the Special Structures Generated for the 16-atom ($Ga_{12}Zn_4$) and ($N_{12}O_4$) Unit Cells

	random	SQS-16[a]	S_a	S_b	S_c
$\bar{\Pi}_{2,1}$	0.25	0.25	0.25	0.25	0.25
$\bar{\Pi}_{2,1}$	0.25	0.25	0.33333	0.16667	0
$\bar{\Pi}_{2,2}$	0.25	0.25	0.25	0.25	0.25
$\bar{\Pi}_{2,3}$	0.25	0.25	0	0	0
$\bar{\Pi}_{2,4}$	0.25	0.25	0.25	0.25	0.25
$\bar{\Pi}_{2,4}$	0.25	0.45833	0.33333	0.16667	0
$\bar{\Pi}_{2,5}$	0.25	0.33333	0	0.16667	0.33333

[a] Reference 22.

TABLE 3: GGA+*U* Calculated Lattice Parameters *a*, *b*, *c* (in Å), Total Energies E_{tot} (in eV), and Cohesive Energies E_{coh} (in eV) of the 32-Atom ($Ga_{12}Zn_4$)($N_{12}O_4$) Supercell

	a	*b*	*c*	E_{tot}	E_{coh}
S_a::S_a	3.186	3.186	5.165	−186.226	8.641
S_b::S_b	3.181	3.181	5.160	−187.004	8.690
S_c::S_c	3.175	3.175	5.155	−187.807	8.740

phase segregation. The lattice parameter *a* shows a small degree of deviation from the ideal behavior, while the lattice parameter *c* exhibits a significant upward bowing. Experimentally for zinc concentration $x < 0.25$,[12] the *a*-axis length of the ($Ga_{1-x}Zn_x$)($N_{1-x}O_x$) solid solution is found to increase almost linearly with increasing zinc concentration, *x*, while the *c*-axis length deviates slightly from this linear relationship. We see that our results in this concentration range exhibit a larger deviation for both lattice parameters, compared to experimental findings.

32-Atom ($Ga_{16-n}Zn_n$)($N_{16-n}O_n$) Supercell. To study the effect of different supercell sizes, in this section, we present our results for a larger 32-atom ($Ga_{16-n}Zn_n$)($N_{16-n}O_n$) supercell. For the low $x = 0.0625$ (and high $x = 0.9375$) concentration limits, we have used the "impurity supercell" approach with only one Zn−O or Ga−N pair per cell and studied two different configurations. We found that similar to the 16-atom ($Ga_{8-n}Zn_n$)($N_{8-n}O_n$) supercell the C_a configuration (with the anion being above the first-nearest-neighbor cation along the *c* axis) is energetically more favorable (∼0.1 eV) than the C_b configuration. For concentrations $x = 0.25$, 0.5, and 0.75, we have adopted the two-step approach detailed in the Model and Method Section and the results are presented below.

Crystal Structures of ($Ga_{0.75}Zn_{0.25}$)($N_{0.75}O_{0.25}$). To construct model structures for the ($Ga_{0.75}Zn_{0.25}$)($N_{0.75}O_{0.25}$) solid solution, we need to first generate special structures for the ($Ga_{0.75}Zn_{0.25}$) and ($N_{0.75}O_{0.25}$) hcp sublattices. The schematic descriptions of the three 16-atom special structures for the ($Ga_{0.75}Zn_{0.25}$) hcp sublattice, S_a, S_b, and S_c, which have pair correlation functions that best match those of the random $Ga_{0.75}Zn_{0.25}$ hcp alloy, are shown in Figure S1 in the Supporting Information. A similar set of special structures can also be obtained for the ($N_{0.75}O_{0.25}$) hcp sublattice (shown in Figure S2) because the two sublattices are related by the internal parameter *u* along the *c* axis. This set of special structures is also denoted as S_a, S_b, and S_c, and combinations of the special structures for the cation and anion hcp sublattices as S_a::S_a, S_b::S_b, and S_c::S_c. Table 2 lists the pair correlation functions up to the fifth-nearest neighbor of our special structures. For comparison, results for the random alloy and those from ref 22 for the 16-atom SQS with ideal *c*/*a* ratio ($\sqrt{8/3} \cong 1.633$) are also listed here. Note that the structural descriptions of our special structures are different from those of the SQS-16 structure from ref 22. First, the *c*/*a* ratio of all of our structures is chosen to be 1.627, which is the value of the pure GaN bulk from our GGA+*U* calculation (see Table 1). Second, all of our structures have hexagonal symmetry with the lattice parameters being twice those of the pure GaN bulk and the atomic positions corresponding to the fractional coordinates of the 16 Ga atoms in the 2 × 2 × 2 GaN wurtzite lattice.

TABLE 4: Pair Correlation Functions up to the Fifth Neighbor of the Generated Special Structures for the 16-Atom (Ga_8Zn_8) and (N_8O_8) Unit Cells

	random	SQS-16[a]	S_a	S_b	S_c
$\bar{\Pi}_{2,1}$	0	0	0	0	−0.333
$\bar{\Pi}_{2,1}$	0	0	0	0	−0.333
$\bar{\Pi}_{2,2}$	0	0	0	0	1.0
$\bar{\Pi}_{2,3}$	0	0	0	−1.0	1.0
$\bar{\Pi}_{2,4}$	0	0	0	0	−0.333
$\bar{\Pi}_{2,4}$	0	0	0	0	−0.333
$\bar{\Pi}_{2,5}$	0	0	−0.333	0	1.0
$\bar{\Pi}_{2,6}$	0	−0.33333	1.0	1.0	−0.333
$\bar{\Pi}_{2,7}$	0	0	0	0	−0.333

[a] Reference 22.

TABLE 5: GGA+*U* Calculated Lattice Parameters *a*, *b*, *c* (in Å), Total Energies E_{tot} (in eV), and Cohesive Energies E_{coh} (in eV) of the 32-Atom (Ga_8Zn_8)(N_8O_8) Supercell

	a	*b*	*c*	E_{tot}	E_{coh}
S_a::S_a	3.202	3.202	5.174	−170.944	8.121
S_b::S_b	3.206	3.206	5.163	−170.878	8.117
S_c::S_c	3.191	3.191	5.194	−171.402	8.150

As we can see from Table 2, while the SQS-16 structure from ref 22 represents the random alloys quite well up to the third-nearest neighbor, our three special structures cannot satisfy the pair correlation functions of random alloys even for the first-nearest-neighbor pair. Note that there are two entries for $\bar{\Pi}_{2,1}$ and $\bar{\Pi}_{2,4}$ (notation from ref 22) in Table 2, which are for pairs that are crystallographically inequivalent but have the same interatomic distance. For our special structures with nonideal *c*/*a* ratios, there is a slight difference between the interatomic distances for these pairs, and as a result, the calculated pair correlation functions are also different. Results for the (Ga_4Zn_{12}) and (N_4O_{12}) unit cells are the same because their structures are simply obtained by switching the Ga and Zn (N and O) atoms in the special structures for ($Ga_{12}Zn_4$) and ($N_{12}O_4$).

Figure 3 shows the fully relaxed configurations of the ($Ga_{12}Zn_4$)($N_{12}O_4$) supercell using GGA+*U* and combinations of 16-atom special structures for the cation and anion hcp sublattices as initial geometric inputs. The corresponding lattice parameters of the scaled unit cells, the total energies, and the cohesive energies are listed in Table 3. By switching the Ga and Zn atoms and the N and O atoms, one can obtain three similar special configurations of the (Ga_4Zn_{12})(N_4O_{12}) supercell approximately. As we can see here, a combination of S_c structures for the cation and anion gives the most stable configuration of the ($Ga_{12}Zn_4$)($N_{12}O_4$) supercell. Compared to the other two configurations, the S_c::S_c configuration is more symmetric and overall closer to the hexagonal wurtzite structure. In this configuration, each cation (Ga or Zn) is coordinated with four anions (N or O) and vice versa. However, some of the Zn and O atoms are undercoordinated in both the S_a::S_a and S_b::S_b configurations because of the significant relaxation of their lattice parameters and atomic positions. Note that the relative atomic positions of the S_c::S_c configuration are quite similar to those of the most stable configuration of the 16-atom (Ga_6Zn_2)-(N_6O_2) supercell (Figure 1b).

Crystal Structures of ($Ga_{0.5}Zn_{0.5}$)($N_{0.5}O_{0.5}$). Table 4 lists the pair correlation functions up to the seventh-nearest neighbor of the two 16-atom special structures of ($Ga_{0.5}Zn_{0.5}$) and ($N_{0.5}O_{0.5}$) hcp sublattices, S_a and S_b, that best match the

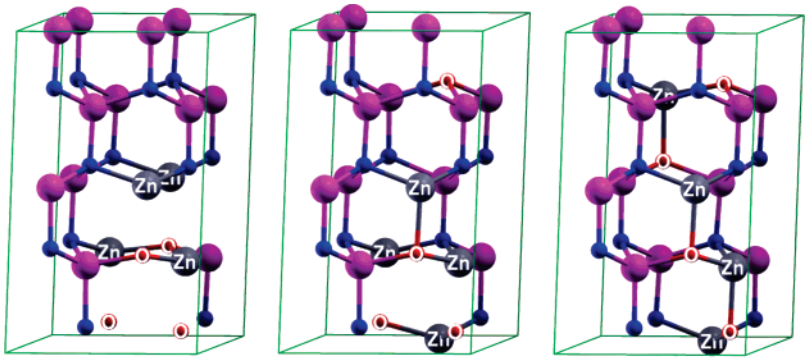

Figure 3. Fully relaxed configurations of the 32-atom $(Ga_{12}Zn_4)(N_{12}O_4)$ supercell using combinations of the 16-atom special structures for the cation and anion hcp sublattices as initial geometric inputs: Ga (purple), N (blue), Zn (gray), and O (red).

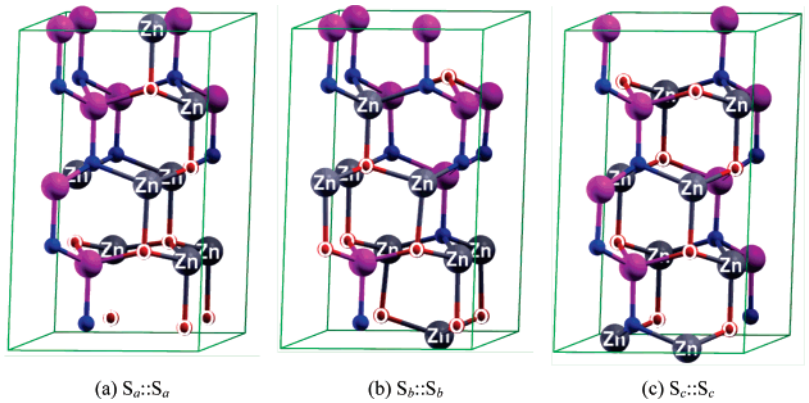

Figure 4. Fully relaxed configurations of 32-atom $(Ga_8Zn_8)(N_8O_8)$ using combinations of the three 16-atom special structures as initial geometric inputs: Ga (purple), N (blue), Zn (gray), and O (red).

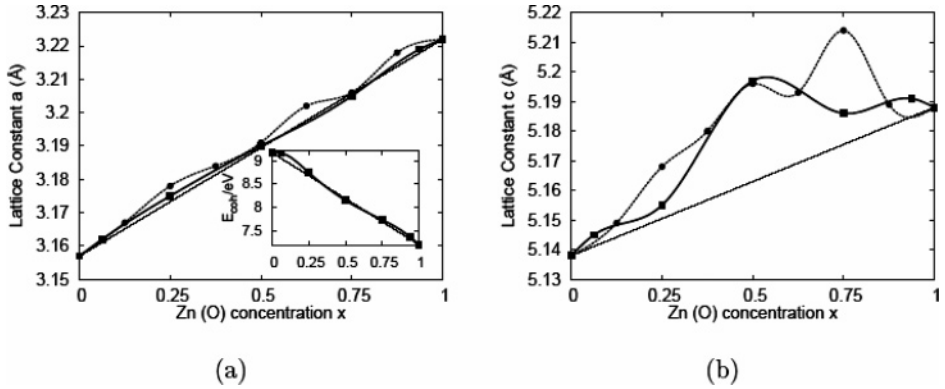

Figure 5. Calculated lattice parameters *a* (a) and *c* (b) of the modified unit cell for the most stable configurations of the 32-atom $(Ga_{16-n}Zn_n)(N_{16-n}O_n)$ (squares) supercell as a function of Zn (O) concentration, *x*. Results for the 16-atom $(Ga_{8-n}Zn_n)(N_{8-n}O_n)$ supercell (circles) are also shown here for comparison. The inset shows the corresponding cohesive energies per formula unit at each *x*.

correlation functions of a random $A_{0.5}B_{0.5}$ hcp alloy. The results from ref 22 for a 16-atom SQS of a $A_{0.5}B_{0.5}$ hcp binary alloy are also listed here. We see that our special S_a and S_b structures can satisfy the random correlation function up to the fourth- and second-nearest neighbor, respectively. However, the atomic arrangements of the combined unrelaxed S_a::S_a and S_b::S_b structures are quite different from that of the most stable configuration of the 16-atom $(Ga_4Zn_4)(N_4O_4)$ supercell. So, for comparison, we have also constructed a structure S_c that has an atomic arrangement similar to the most stable configuration of the eight-atom (Ga_4Zn_4) and (N_4O_4) unit cells and has twice the size of these unit cells along the *c* axis. The pair correlation functions of the S_c structure are also listed in Table 4, and, as can be seen here, this structure does not satisfy the random correlation function even for the first-nearest-neighbor pair. The schematic descriptions of these 16-atom special structures for both hcp sublattices are shown in Figures S3 and S4 in the Supporting Information.

The fully relaxed configurations of the $(Ga_8Zn_8)(N_8O_8)$ supercell are shown in Figure 4, and the corresponding structural properties are presented in Table 5. We see that there are two undercoordinated Zn and O atoms in the S_a::S_a combination while every atom in both the S_b::S_b and S_c::S_c configurations has a coordination of four atoms. The fully relaxed structures for both S_b::S_b and S_c::S_c combinations have lattice parameters that are consistent with a hexagonal wurtzite lattice; however, the atomic positions in both structures are displaced from their ideal positions because of local relaxation. Overall, the relaxed S_c::S_c configuration is found to be closer to the regular

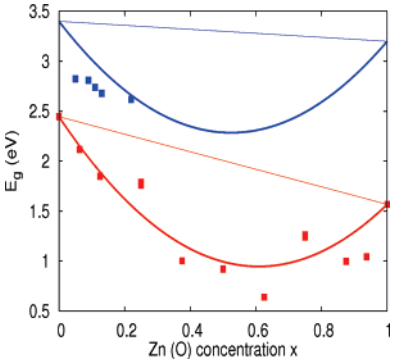

Figure 6. Variation of band gap as a function of Zn (O) concentration, x. Red squares: calculated band gaps of the most stable configurations of the 16-atom $(Ga_{8-n}Zn_n)(N_{8-n}O_n)$ and 32-atom $(Ga_{16-n}Zn_n)(N_{16-n}O_n)$ supercells at different x; red curve: smoothed $E_g(x)$ curve using the estimated bowing parameter b; blue squares: experimental data for $(Ga_{1-x}Zn_x)(N_{1-x}O_x)$ solid solution from ref 12; blue curve: predicted experimental $E_g(x)$ behavior using the estimated b and the limiting GaN and ZnO band gaps from ref 12; red and blue straight lines: ideal solution behavior for the calculated and experimental band gaps.

hexagonal wurtzite structure and more stable than the S_b::S_b configuration.

Variation of Structural Properties with x. Figure 5 shows the variations of the lattice parameters a and c of the scaled unit cell with Zn (O) concentration, x for the 32-atom $(Ga_{16-n}Zn_n)(N_{16-n}O_n)$ supercell (squares). For comparison, results for the 16-atom $(Ga_{8-n}Zn_n)(N_{8-n}O_n)$ supercell (circles) are also shown here. The corresponding cohesive energies per formula unit are shown in the inset. We see that again the calculated cohesive energy E_{coh} shows a nearly linear variation versus Zn (O) concentration, x. The lattice parameter a shows a smaller degree of deviation from linear interpolation, almost ideal behavior, compared to the results for the 16-atom $(Ga_{8-n}Zn_n)(N_{8-n}O_n)$ supercell. The lattice parameter c still exhibits a significant upward bowing, although it is now in better agreement with experimental findings for zinc concentration $x < 0.25$.[12] The calculated lattice mismatch between GaN and ZnO is about 2.0% for a and 1.0% for c. The smaller difference in c might be responsible for the significant deviation from the ideal behavior.

Electronic Properties of $(Ga_{1-x}Zn_x)(N_{1-x}O_x)$ Solid Solution. For a given concentration, x, we have performed electronic band structure calculations for both supercells using the fully relaxed structures. The calculated band gap is found to be very sensitive to the choice of the supercell configuration. Take the 32-atom $(Ga_{12}Zn_4)(N_{12}O_4)$ supercell, for example. We obtain a band gap of 1.79 eV for the most stable S_c::S_c structure, but only 0.74 eV for the less stable S_b::S_b structure. For the 32-atom $(Ga_8Zn_8)(N_8O_8)$ supercell, partial occupancy of the conduction band minimum is found for the two less stable (S_a::S_a and S_b::S_b) structures. In Figure 6, we plot the calculated band gaps E_g using the most stable configurations as a function of Zn (O) concentration, x, for both the 16-atom $(Ga_{8-n}Zn_n)(N_{8-n}O_n)$ and 32-atom $(Ga_{16-n}Zn_n)(N_{16-n}O_n)$ supercells. Owing to the use of the empirical U correction, our calculated band gaps are qualitatively correct, although still underestimated, compared to the experimental values. Note that both supercells give almost identical band gaps for concentration $x = 0.25$, 0.5, and 0.75.

Although there is scatter in the calculated band gaps owing to the finite size of the supercells employed, over the entire composition range we see that the band gap, E_g, exhibits a downward bowing for both supercells, which suggests that there is a minimum band gap for the solid solution at some intermediate Zn (O) concentration. The composition dependence of $E_g(x)$ and the observed optical bowing for binary $A_{1-x}B_x$ and ternary $A_{1-x}B_xC$ semiconductor alloys have been studied theoretically in attempts to find a simple relation between these quantities.[19,43−45] For binary $A_{1-x}B_x$ alloys, the band gap $E_g(x)$ can be described by[19,45]

$$E_g(x) = (1 - x)E_g(A) + xE_g(B) - bx(1 - x) \qquad (3)$$

where b is an optical bowing parameter. For our pseudobinary $(Ga_{1-x}Zn_x)(N_{1-x}O_x)$ solid solution, this bowing parameter can be estimated via a least-squares fit of eq 3 to the combined data (red solid squares in Figure 6) obtained for the 16-atom $(Ga_{8-n}Zn_n)(N_{8-n}O_n)$ and 32-atom $(Ga_{16-n}Zn_n)(N_{16-n}O_n)$ supercells at various Zn (O) concentrations, x. The optimum bowing parameter is thus determined to be 4.050, and the resulting smoothed $E_g(x)$ curve is also shown in red in Figure 6. Using experimental limiting (pure GaN and ZnO) band gap values published in ref 12 instead of our calculated ones and our estimated bowing parameter, the experimental $E_g(x)$ behavior of the $(Ga_{1-x}Zn_x)(N_{1-x}O_x)$ solid solution is predicted to follow the downward-bowed curve shown in blue in Figure 6. We see that again our results are in qualitative agreement with experimental findings (blue solid squares) for concentration $x < 0.25$. The minimum band gap is estimated to be about 2.29 eV at $x = 0.525$, suggesting that the photocatalytic activity of this solid solution may be further improved by increasing Zn (O) concentration, x.

DOS and Band Structure Analysis of the Observed Band-Gap Narrowing. We now look at the variation of the electronic bands of the 32-atom $(Ga_{16-n}Zn_n)(N_{16-n}O_n)$ supercell with Zn (O) concentration, x. This can provide us with information about the relationship between x and the nature of the lower conduction bands and the upper valence bands of the $(Ga_{1-x}Zn_x)(N_{1-x}O_x)$ solid solution and the resulting band gap behavior. Figure 7 shows the partial DOS of the anion (N and O) 2p states in the upper valence bands and the cation (Ga and Zn) 4s and 4p states in the lower conduction bands as a function of concentration, x. The partial DOS of the cation (Ga and Zn) 3d states are also plotted there to illustrate the contribution of the 2p−3d coupling in the upper valence bands. Two interesting features can be seen from Figure 7.

First, we see that for all $(Ga_{1-x}Zn_x)(N_{1-x}O_x)$ solid solutions ($0.0625 \le x \le 0.9375$) the top of the valence band always consists of N 2p states followed by O 2p and Zn 3d states, while the bottom of the conduction band *appears* to switch from Ga 4s and 4p ($x \le 0.5$) to Zn 4s and 4p (see further discussion of this point below). Second, we see that the Ga 3d states are located 15−17 eV below the Fermi energy level of each system and are well separated from both N and O 2p states. In contrast, the Zn 3d states sit just 7−9 eV below each Fermi energy level and are very energetically close to the N and O 2p states. This close proximity in energy leads to very strong 2p−3d coupling. Note that the bandwidth of the Ga 3d states becomes narrower as x increases, while that of Zn 3d states broadens.

Figure 8 shows the calculated band structure of the $(Ga_{1-x}Zn_x)(N_{1-x}O_x)$ solid solution at $x = 0.5$, the discrete composition closest to the predicted minimum of the band gap. It is clear from the figure that the minimum band gap occurs at the Γ point where the bottom of the conduction band consists of a single, isolated band. The band character analysis of this lowest conduction band as a function of Zn (O) concentration is shown in Figure 9, where the N "3s" and O "3s" signifiy a spherically symmetric density centered on O and N, respectively. These "3s" components of the partial DOS are too small to be

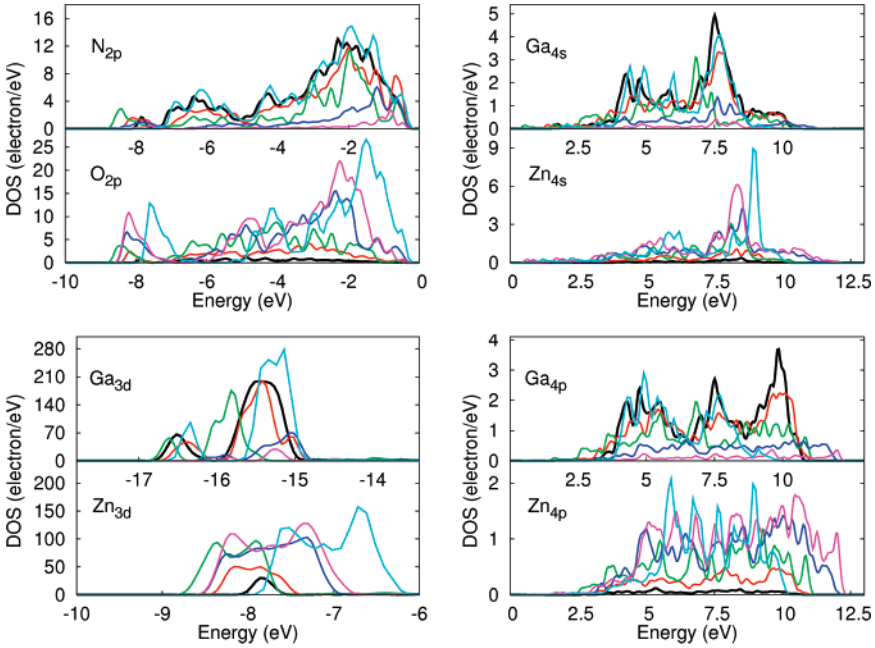

Figure 7. Partial density of states (DOS) of the 32-atom $(Ga_{16-n}Zn_n)(N_{16-n}O_n)$ supercell as a function of Zn (O) concentration, x. Energies are specified to the Fermi level of the supercell at each concentration, x. In all subfigures, $x = 0.0625$ (black); 0.25 (red); 0.5 (green); 0.75 (blue); 0.9375 (magenta); 0.0 or 1.0 (cyan).

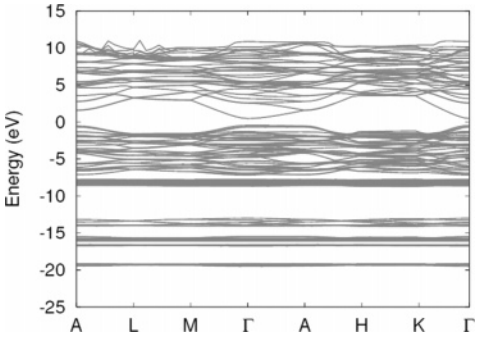

Figure 8. Calculated band structure of the $(Ga_{1-x}Zn_x)(N_{1-x}O_x)$ solid solution with the 32-atom supercell for $x = 0.5$.

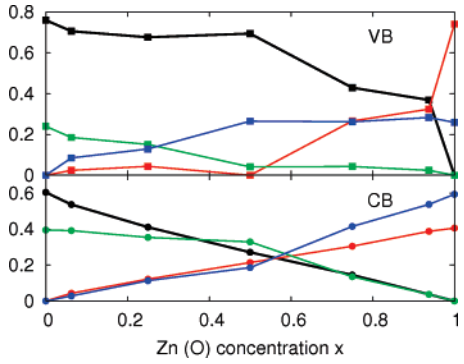

Figure 9. Band character analysis (relative contributions from N, O, Ga, and Zn atoms) of the highest valence band (VB, top panel, squares) and lowest conduction band (CB, bottom panel, circles) at the Γ point as a function of Zn (O) concentration, x. Lines connecting points are just the guides for the eye. In the top panel: black squares, N 2p; red squares, O 2p; green squares, Ga 3d; and blue squares, Zn 3d. In the bottom panel: black circles, N "3s"; red circles, O "3s"; green circles, Ga 4s and 4p; and blue circles, Zn 4s and 4p.

clearly seen when considering the entire conduction band as in Figure 7. Also shown in Figure 9 is the band character analysis of the top band of the valence band at the Γ point. Consistent with the discussion regarding Figure 7, the character of the top of the valence band is dominated by N 2p at all Zn (O) concentrations except those approaching unity, where it becomes dominated by O 2p. The larger contribution of Zn 3d over O 2p for $x < 0.75$ is unexpected and may arise from limitations of the Zn 3d on-site Coulomb interaction correction, U. The bottom of the conduction band is composed primarily of N "3s" with some Ga 4s and 4p at $x < 0.25$ and of Zn 3d with some O "3s" for $x > 0.75$. In the region of the minimum of the band gap ($x = 0.525$), the character of the bottom of the conduction band is delocalized over all of the constituent elements of the solid solution. Such delocalization would likely stabilize the bottom of the conduction band at these compositions, thereby narrowing the band gap.

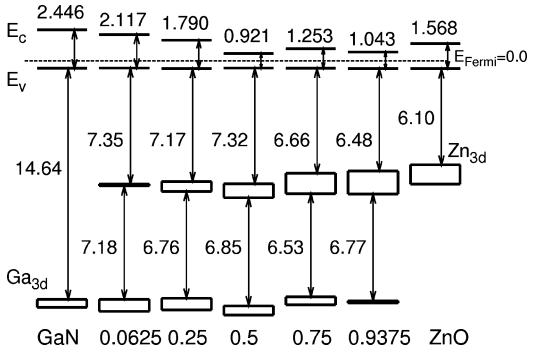

Figure 10. Diagram of calculated band positions and band gaps of the 32-atom $(Ga_{16-n}Zn_n)(N_{16-n}O_n)$ supercell as a function of Zn (O) concentration, x. Band energies are specified relative to the Fermi level at each concentration, x. Here E_v is the valence band maximum and E_c is the conduction band minimum. The energy ranges of the Zn and Ga 3d bands are indicated by boxes.

Figure 10 shows a diagram of the calculated band positions and band gaps of the 32-atom $(Ga_{16-n}Zn_n)(N_{16-n}O_n)$ supercell versus Zn (O) concentration, x. Energies here as in Figures 7 and 8 are specified relative to the Fermi level of the 32-atom supercell at each concentration, x. Similar results are also obtained for the 16-atom $(Ga_{8-n}Zn_n)(N_{8-n}O_n)$ supercell and thus are not shown here.

As seen in Figure 10, the Zn 3d states move upward with respect to E_v, the top of the valence band, for $x > 0.5$ while the

shift in the Ga 3d states is very small as x increases. More importantly, we see that relative to the Fermi level of the 32-atom $(Ga_{16-n}Zn_n)(N_{16-n}O_n)$ supercell at each concentration, x, the shift in the valence band maximum, E_v, is negligible while the conduction band minimum, E_c, moves first downward ($x \leq 0.5$) and then upward. As a result, the overall band gap is lower than those of the pure components (GaN and ZnO) and exhibits a downward bowing behavior over the entire composition region. The optical bowing in semiconductor ternary alloys has been studied extensively by Zunger et al., and the mechanism has been attributed to contributions from the volume deformation due to the compression and/or dilation of binary constituents into the alloy's volume and the structural relaxations in going from the unrelaxed to the fully relaxed configurations.[45,46] Such structural relaxations may be responsible for the change in character and delocalization of the bottom of the conduction band seen in Figure 9. For our pseudobinary solid solution, we suggest that these structural contributions, as well as the strong 2p−3d coupling between Zn and N (O) atoms, contribute significantly to the observed band gap bowing.

Conclusions

We have conducted a systematic study of the structural and electronic properties of $(Ga_{1-x}Zn_x)(N_{1-x}O_x)$ solid solutions using density-functional theory. The GGA+U approach has been employed, and our calculated band gaps are qualitatively correct, although still underestimated, compared to the experimental values. The composition dependence of these properties has been investigated using the periodic structure approach. Both 16-atom $(Ga_{8-n}Zn_n)(N_{8-n}O_n)$ and 32-atom $(Ga_{16-n}Zn_n)(N_{16-n}O_n)$ supercells have been considered, and the special quasirandom structures approach has been adopted for the 32-atom supercell to construct model structures. We found that although the most stable configuration does not necessarily correspond to the structures that best represent the random cation and anion sublattices this approach greatly reduces computational costs and provides useful benchmark structures. For the lower concentration range ($x < 0.25$), our results for both supercells are in qualitative agreement with experimental findings, although overall the larger 32-atom supercell provides a better description for the solid solution. Moreover, we have observed downward bowing of the band gap over the entire composition range, and the minimum band gap is estimated to be about 2.29 eV for concentration $x = 0.525$. This suggests that the photocatalytic activity of this solid solution can be further improved by increasing the zinc (oxygen) concentration. The observed band gap behavior is investigated via analysis of the density of states and the band positions of this solid solution. The strong 2p−3d coupling between Zn and N (O) atoms and contributions from the volume deformation and the structural relaxations causing delocalization of the bottom of the conduction band are suggested to be responsible for the overall band gap behavior.

Acknowledgment. This work is performed at Brookhaven National Laboratory under contract DE-AC02-98CH10886 with the U.S. Department of Energy and supported by its Division of Chemical Sciences, Geosciences, & Biosciences; Office of Basic Energy Sciences. J.T.M. gratefully acknowledges helpful discussions with Mark Hybertsen. L.L.J. thanks Zi-Kui Liu at The Pennsylvania State University for helpful discussions about the special quasirandom structures approach. The ball-and-stick graphs were generated using XCrySDen graphical package.[47] The code is available from http://www.xcrysden.org/.

Supporting Information Available: Schematic descriptions of the generated special structures for the $(Ga_{0.75}Zn_{0.25})$, $(Ga_{0.5}Zn_{0.5})$, $(N_{0.75}O_{0.25})$, and $(N_{0.5}O_{0.5})$ hcp sublattices and coordinates of key structures. This material is available free of charge via the Internet at http://pubs.acs.org.

References and Notes

(1) Bak, T.; Nowotny, J.; Rekas, M.; S. C. C. *Int. J. Hydrogen Energy* **2002**, *27*, 991.
(2) Fujishima, A.; Honda, K. *Nature* **1972**, *238*, 37.
(3) Kim, H. G.; Hwang, D. W.; Kim, J.; Kim, Y. G.; Lee, J. S. *Chem. Commun.* **1999**, 1077.
(4) Dhanalakshmi, K. B.; Latha, S.; Anandan, S.; Maruthamuthu, P. *Int. J. Hydrogen Energy* **2001**, *26*, 669.
(5) Zou, Z.; Ye, J.; Sayama, K.; Arakawa, H. *Nature* **2001**, *414*, 625.
(6) Kim, H. G.; Borse, P. H.; Choi, W.; Lee, J. S. *Angew. Chem., Int. Ed.* **2005**, *44*, 4585.
(7) Bae, E.; Choi, W. *J. Phys. Chem. B* **2006**, *110*, 14792.
(8) Dürr, M.; Rosselli, S.; Yasuda, A.; Nelles, G. *J. Phys. Chem. B* **2006**, *110*, 21899.
(9) Maeda, K.; Takata, T.; Hara, M.; Saito, N.; Inoue, Y.; Kobayashi, H.; Domen, K. *J. Am. Chem. Soc.* **2005**, *127*, 8286.
(10) Maeda, K.; Teramura, K.; Lu, D. L.; Takata, T.; Saito, N.; Inoue, Y.; Domen, K. *Nature* **2006**, *440*, 295.
(11) Yashima, M.; Maeda, K.; Teramura, K.; Takata, T.; Domen, K. *Chem. Phys. Lett.* **2005**, *416*, 225.
(12) Maeda, K.; Teramura, K.; Takata, T.; Hara, M.; Saito, N.; Toda, K.; Inoue, Y.; Kobayashi, H.; Domen, K. *J. Phys. Chem. B* **2005**, *109*, 20504.
(13) Schröer, P.; Krüger, P.; Pollmann, J. *Phys. Rev. B* **1993**, *47*, 6971.
(14) Lagerstedt, O.; Monemar, B. *Phys. Rev. B* **1979**, *19*, 3064.
(15) Kocha, S. S.; Peterson, M. W.; Arent, D. J.; Redwing, J. M.; Tischler, M. A.; Turner, J. A. *J. Electrochem. Soc.* **1995**, *142*, L238.
(16) Beach, J. D.; Collins, R. T.; Turner, J. A. *J. Electrochem. Soc.* **2003**, *150*, A899.
(17) Li, S.; Ouyang, C. *Phys. Lett. A* **2005**, *336*, 145.
(18) Wei, S.-H.; Ferreira, L. G.; Bernard, J. E.; Zunger, A. *Phys. Rev. B* **1990**, *42*, 9622.
(19) Wei, S.-H.; Zunger, A. *Phys. Rev. Lett.* **1996**, *76*, 664.
(20) Gan, C. K.; Feng, Y. P.; Srolovitz, D. J. *Phys. Rev. B* **2006**, *73*, 235214.
(21) Jiang, C.; Wolverton, C.; Sofo, J.; Chen, L.-Q.; Liu, Z.-K. *Phys. Rev. B* **2004**, *69*, 214202.
(22) Shin, D.; Arróyave, R.; Liu, Z.-K. *Phys. Rev. B* **2006**, *74*, 024204.
(23) Wei, S.-H.; Zunger, A. *Phys. Rev. B* **1988**, *37*, 8958.
(24) Van de Walle, C. G.; Neugebauer, J. *Appl. Phys. Lett.* **1997**, *70*, 2577.
(25) Lichtenstein, A. I.; Anisimov, V. I.; Zaanen, J. *Phys. Rev. B* **1995**, *52*, R5467.
(26) Anisimov, V. I.; Aryasetiawan, F.; Lichtenstein, A. I. *J. Phys.: Condens. Matter* **1997**, *9*, 767.
(27) Erhart, P.; Albe, K.; Klein, A. *Phys. Rev. B* **2006**, *73*, 205203.
(28) Filippetti, A.; Spaldin, N. A. *Phys. Rev. B* **2003**, *67*, 125109.
(29) Oshikiri, M.; Aryasetiawan, F. *Phys. Rev. B* **1999**, *60*, 10754.
(30) van de Walle, A.; Asta, M.; Ceder, G. *CALPHAD: Comput. Coupling Phase Diagrams Thermochem.* **2002**, *26*, 539.
(31) Kresse, G.; Joubert, D. *Phys. Rev. B* **1999**, *59*, 1758.
(32) Perdew, J. P.; Burke, K.; Ernzerhof, M. *Phys. Rev. Lett.* **1996**, *77*, 3865.
(33) Perdew, J. P.; Chevary, J. A.; Vosko, S. H.; Jackson, K. A.; Pederson, M. R.; Singh, D. J.; Fiolhais, C. *Phys. Rev. B* **1991**, *46*, 6671.
(34) Kresse, G.; Furthmuller, J. *Comput. Mater. Sci.* **1996**, *6*, 15.
(35) Janotti, A.; Segev, D.; Van de Walle, C. G. *Phys. Rev. B* **2006**, *74*, 045202.
(36) Nakamura, K.; Arita, R.; Yoshimoto, Y.; Tsuneyuki, S. *Phys. Rev. B* **2006**, *74*, 235113.
(37) Chanier, T.; Sargolzaei, M.; Opahle, I.; Hayn, R.; Koepernik, K. *Phys. Rev. B* **2006**, *73*, 134418.
(38) Dong, C. L.; Persson, C.; Vayssieres, L.; Augustsson, A.; Schmitt, T.; Mattesini, M.; Ahuja, R.; Chang, C. L.; Guo, J.-H. *Phys. Rev. B* **2004**, *70*, 195325.
(39) Dudarev, S. L.; Botton, G. A.; Savrasov, S. Y.; Humphreys, C. J.; Sutton, A. P. *Phys. Rev. B* **1998**, *57*, 1505.
(40) Leszczynski, M.; Teisseyre, H.; Suski, T.; Grzegory, I.; Bockowski, M.; Jun, J.; Porowski, S.; Pakula, K.; Baranowski, J. M.; Foxon, C. T.; Cheng, T. S. *Appl. Phys. Lett.* **1996**, *69*, 73.
(41) Karzel, H.; Potzel, W.; Köfferlein, M.; Schiessl, W.; Steiner, M.; Hiller, U.; Kalvius, G. M. *Phys. Rev. B* **1996**, *53*, 11425.
(42) Desgreniers, S. *Phys. Rev. B* **1998**, *58*, 14102.
(43) Zunger, A.; Jaffe, J. E. *Phys. Rev. Lett.* **1983**, *51*, 662.
(44) Bernard, J. E.; Zunger, A. *Phys. Rev. B* **1987**, *36*, 3199.
(45) Wei, S.-H.; Zunger, A. *J. Appl. Phys.* **1995**, *78*, 3846.
(46) Magri, R.; Froyen, S.; Zunger, A. *Phys. Rev. B* **1991**, *44*, 7947.
(47) Kokalj, A. *Comput. Mater. Sci.* **2003**, *28*, 155.